A New Method for Generating a Global Forest Aboveground Biomass Map From Multiple High-Level Satellite Products and Ancillary Information

Lu Yang, Shunlin Liang, *Fellow, IEEE*, and Yuzhen Zhang

***Abstract*—Global forest aboveground biomass (AGB) is very important in quantifying carbon stock, and, therefore, it is necessary to estimate forest AGB accurately. Many studies have obtained reliable AGB estimates by using light detection and ranging (LiDAR) data. However, it is difficult to obtain LiDAR data continuously at regional or global scale. Although many studies have integrated multisource data to estimate biomass to compensate for these deficiencies, few methods can be applied to produce global time series of high-resolution AGB due to the complexity of the method, data source limitations, and large uncertainty. This study developed a new method to produce a global forest AGB map using multiple data sources—including LiDAR-derived biomass products, a suite of high-level satellite products, forest inventory data, and other auxiliary datasets—to train estimated models for five different forest types. We explored three machine learning methods [artificial neural network, multivariate adaptive regression splines, and gradient boosting regression tree (GBRT)] to build the estimated models. The GBRT method was the optimal algorithm for generating a global forest AGB map at a spatial resolution of 1 km. The independent validation result showed good accuracy with an R^2 value of 0.90 and a root mean square error value of 35.87 Mg/ha. Moreover, we compared the generated global forest AGB map with several other forest AGB maps and found the results to be highly consistent. An important feature of this new method is its ability to produce time series of high-resolution global forest AGB maps because it heavily relies on high-level satellite products.**

***Index Terms*—Biomass, global, machine learning, multiple satellite products.**

I. Introduction

THE largest ecosystem on the earth is the forest, which is the main carbon sink [1]. Changes in forests can lead to a series of environmental and climate changes [2]–[4]. Therefore, effective long-term monitoring of forest biomass in space is necessary. For forest biomass, because of the difficulty measuring belowground biomass (BGB), most studies focus on aboveground biomass (AGB) [5], which accounts for a large proportion of total forest biomass. The BGB was usually calculated based on AGB by the conversion ratio. Therefore, in this article, we only focus on forest AGB estimating.

Presently, the methods of estimating forest biomass can be divided into three categories: the measured-based methods, the model-based simulation methods, and the remote sensing-based methods [6]–[10]. Since remote sensing technology can obtain a wide range of data quickly, lots of studies have used different remote sensing data and field data to estimate forest AGB by using different algorithms at a regional scale [11]–[14]. Although lots of studies can get reliable estimates of the forest AGB, few methods can generate a time-series global forest AGB data. Hence, the development of a method to generate a time-series global forest AGB data is important.

Trees absorb carbon dioxide (CO_2) from the atmosphere and use photosynthetically active radiation to convert the CO_2 into organic matter through photosynthesis. In the process of trees accumulation biomass, many structural parameters are closely related to biomass. Leaf area index (LAI) is an important parameter for quantitative analysis of trees growth and photosynthesis processes, and is also the primary parameter in many ecosystem models [15], [16] and forest AGB estimation [17], [18]. In addition, the net primary productivity (NPP) reflects the forest over time accumulated huge amounts of carbon, which is the amount of organic carbon stocked by photosynthesis. Numerous studies have confirmed that NPP has a certain correlation with forest AGB [19], [20]. Directly using gross primary productivity (GPP) instead of using NPP may avoid the propagation error, because the NPP cannot directly be obtained by remote sensing. Additionally, the canopy height can describe the vertical information of the forest, which is a key parameter used to estimate forest AGB and can reduce the uncertainty of the prediction [21], especially for areas with high biomass density [22], [23]. Different tree species have different structures and are distributed in different physiognomy and climate regions that have a certain impact on the growth environment of the plants

Manuscript received September 9, 2019; revised January 7, 2020 and February 1, 2020; accepted April 5, 2020. Date of publication May 28, 2020; date of current version June 11, 2020. This work was supported in part by the Chinese Grand Research Program on Climate Change and Response under Grant 2016YFA0600103. *(Corresponding author: Shunlin Liang.)*

Lu Yang is with the College of Urban and Environmental Sciences Key Laboratory for Earth Surface Processes of the Ministry of Education, Peking University, Beijing 100871, China (e-mail: lyang201314@163.com).

Shunlin Liang is with the Department of Geographical Sciences, University of Maryland, College Park, MD 20742 USA (e-mail: sliang@umd.edu).

Yuzhen Zhang is with the School of Automation and Electrical Engineering, University of Science and Technology Beijing, Beijing 100083, China (e-mail: yzhang@ustb.edu.cn).

This article has supplementary downloadable material available at https://ieeexplore.ieee.org, provided by the authors.

Digital Object Identifier 10.1109/JSTARS.2020.2987951

TABLE I
REFERENCE DATA USED IN THIS STUDY

Region	Numbers of plots	Reference
Africa	260	[29]
South America	481	[30, 31]
Asia	18	[31]
Eurasia	1345	[32]
Global	100	[20]
Global	898	[33]
Canada	96	[34]
Global	371	[10]

TABLE II
LiDAR-DERIVED FOREST AGB DATASETS

Region	Spatial resolution	Reference year	Metadata	Reference
North America	500 m	2005–2006	GLAS, SRTM, WWF Ecozone, NLCD	[26]
Eurasia	500 m	2005–2006	ALTM, WWF, GLAS, NLCD	[27]
Tropical	1km	2000	Reference maps, reference field data	[28]

Note: GLAS: Geoscience Laser Altimeter System; SRTM: Shuttle Radar Topography Mission; WWF: World Wildlife Fund; NLCD: National Land Cover Database.

and affect the estimation of the forest AGB [24]. Moreover, the geographic conditions, which have an impact on the soil and climate [24], [25], indirectly affect the growth of forest. Whether the structural parameters of the tree or the environmental and topographic parameters, they can be obtained by remote sensing technology, and lots of them are high-level time-series remote sensing data. Using this rich information to develop the estimate models of forest AGB, the accuracy could be improved. Additionally, this method mainly relied on high-level remote sensing data; therefore, it has the ability to produce time series of high-resolution global forest AGB maps.

The objective of this study was to improve the estimation of global forest AGB by integrating reference data [light detection and ranging (LiDAR)-derived biomass datasets and field measurements], high-level products from remote sensing data (LAI, GPP, VCF, and land cover type), canopy height, climate variables, and topographic data using machine learning technique. To achieve this goal, we built machine learning models for five separate types of forest: Evergreen Needleleaf Forest (ENF), Evergreen Broadleaf Forest (EBF), Deciduous Needleleaf Forest (DNF), Deciduous Broadleaved Forest (DBF), and Mixed Forests (MF). We explored three machine learning methods, including artificial neural network (ANN), multivariate adaptive regression splines (MARS), and gradient boosting regression tree (GBRT). After comparing the performances of these models, we selected the GBRT algorithm to produce the global forest AGB map in 2005. We validated the results using a reference biomass dataset and also compared these results with other AGB maps in numerical and spatial distribution. Additionally, we analyzed the relative importance of covariables at regional and global scales.

II. DATA AND METHODOLOGY

A. Data

1) Reference Dataset: In this study, we collected field data and some LiDAR-based biomass data as reference data. The field data were collected from published papers, as shown in Table I. The LiDAR-based biomass data (see Table II) were mainly from the Oak Ridge National Laboratory Distributed Active Archive Center (ORNL DAAC) [26], [27], which produces many LiDAR biomass datasets with good accuracy and can be download from[1]. LiDAR-based biomass data in tropical forest areas were collected from [28].

To reduce the uncertainty, these reference datasets should be screened by some criteria. Field data should be finely georeferenced; the area of the plot should be larger than 0.05 ha [28], [35]; the average diameter at breast height used to screen the seedling should be larger than 5 cm, and if it has very high biomass value in low VCF value or low biomass value in high VCF value, it should be defined as an outlier. Data should represent the five types of surface cover mentioned earlier. If the field data did not meet these requirements, we removed them. For matching other variables, the field data should be aggregated to a spatial resolution of 1 km by calculating the mean value of the corresponding field data in pixels of 1-km spatial resolution.

In this study, as shown in Table II, we used the LiDAR-derived forest AGB maps over North America and Eurasia from the ORNL DAAC. These LiDAR-derived forest biomass maps were generated by fusing field data, LiDAR data, and other remote sensing data. For tropical forest areas, the forest AGB data presented in [28] was used as the reference data. This dataset integrated two tropical forest AGB maps to generate a more accurate tropical forest AGB dataset with 1-km spatial resolution, as shown in Table II.

Additionally, as Avitabile and Camia [36] suggested, the extremely high value of AGB was abnormal over 1 km^2; hence, for the biomass data (the field data and LiDAR-derived biomass dataset) used in this study, we removed the extreme value, which was higher than the highest datum and lower than the lowest datum.

2) High-Level Satellite Products From Optical Sensors: We selected the Global LAnd Surface Satellite (GLASS) as the source for the LAI and GPP data. GLASS products have been generated from multiple satellite data for long-term environmental change studies [37], [38], and the number of products has increased from the original 5 to 12. The GLASS LAI product [39] has better accuracy and quality compared with other satellite LAI products [40], [41], and its GPP product is based on the light-use efficiency model developed earlier [42]. The GLASS data have a long time series, and its high-precision, global surface, remote sensing products are based on multisource remote sensing data, and ground measured data [38]. These products provide a reliable basis for studying global

[1]Online. [Available]: https://daac.ornl.gov/about/

environmental change and can be widely used in global, intercontinental, and regional dynamic monitoring of atmospheric change and vegetation cover [43]–[45]. Therefore, the satellite products [e.g., GLASS LAI and GPP and Moderate Resolution Imaging Spectroradiometer (MODIS) data], which represent the physical variables of land surfaces and were derived from the low-level products (satellite observed radiance or reflectance), are called high-level satellite products. These products are available on the National Earth System Science Data Sharing Infrastructure[2] and through the University of Maryland Global Land Cover Facility[3].

We collected the VCF and Land Cover Type datasets from the MODIS. The MODIS VCF dataset has 500-m spatial resolution, with annual temporal resolution. In this study, the land cover data product, which was classified based on the IGBP classification standard, can be obtained from the MODIS website[4]. In this study, we built five land-cover-type models, including ENF, EBF, DNF, DBF, and MF models.

3) Topographic Data: The topographic data, a digital elevation model (DEM), is collected from the NASA/NGA SRTM [46]. The DEM data had two different spatial resolutions: one that was 30 m and another that was 90 m. For consistency, we aggregated the DEM with 90-m spatial resolution to a 1-km resolution by resampling. The DEM data can be obtained from[5].

4) Climate Data: In this study, monthly mean temperature and total precipitation data were used as variables to estimate forest AGB [47]. Daily precipitation data were collected from CRU[6], at a spatial resolution of 0.5°, which extended coverage from 90 S to 90 N [48]. We summed this daily information to produce monthly precipitation. The temperature dataset from CRU, with a spatial resolution of 0.5° [48], and the daily temperature were aggregated into monthly mean temperature.

5) Canopy Height: Canopy height has a strong relationship to forest AGB and can provide the vertical information of forest structure. In this study, global canopy height data had 1-km spatial resolution in 2005. The data were from the GLAS aboard Ice, Cloud, and land Elevation Satellite [49]. The canopy height map showed a reasonable correspondence with field data, and the validation results had an R^2 value of 0.49. This canopy height dataset can be obtained from[7].

B. Methodology

Estimating global forest AGB using multisource remote sensing data and auxiliary data consisted of the following three steps, as shown in Fig. 1.

The first step was data preprocessing. Because of the different sources of data used in this study, we had to unify the spatial resolution and geographic projection to reduce the uncertainty caused by geographic location. We unified the datasets used in this study by projecting data into the same geographic projection

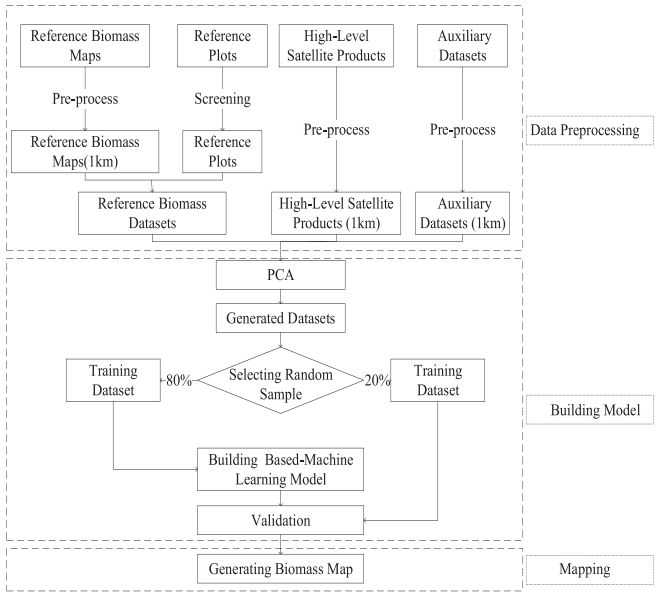

Fig. 1. Flowchart to estimate global forest AGB.

(WGS-84) and then aggregating data to the same spatial resolution (1 km) using the nearest neighbor method. In addition, only the cells with low uncertainty (<10%) were selected from the LiDAR-derived biomass maps as the reference dataset. Because the uncertainty maps were not provided, we used the pixels that corresponded to the training field data as reference data. If the training data and uncertainty map were not provided, the cells were randomly selected from the LiDAR-derived biomass to be the reference data. Furthermore, the LiDAR-derived biomass maps were not directly measured. Therefore, we reduced the difference between the measured data and the LiDAR data by averaging the corresponding measured data within 1 km pixels. Accurate calibration of raw LiDAR data should be done at field plot resolution. But field data was only a small portion of a pixel in this study, we could not do this calibration. Therefore, we just reduced the difference between the measured data and LiDAR data and not calibrated it.

The second step was building the model. In this study, we modeled the five types of land cover (i.e., ENF, EBF, DNF, DBF, and MF) using the same steps. Monthly values for LAI, GPP, precipitation, and temperature and yearly values for VCF, DEM, and canopy height were used as the explanatory variables. To increase computational efficiency and to remove redundant information, we used principal component analysis to reduce the dimensions of the monthly explanatory variables [50] (e.g., LAI, GPP, precipitation, and temperature). After generating the dataset, we randomly selected 80% of its data, as a training dataset, to build models based on the ANN, MARS, and GBRT algorithms. ANN provides a powerful approach for analyzing complicated relationships among variables. MARS is a nonparametric and multivariate regression analysis method, with powerful generalization ability, especially applicable to situations using high-dimensional data [51]. They are widely used in forest AGB estimating [52]. The GBRT method, suggested by

[2]Online. [Available]: http://www.geodata.cn
[3]Online. [Available]: http://glcf.umd.edu/
[4]Online. [Available]: https://modis.gsfc.nasa.gov
[5]Online. [Available]: http://www.cgiar-csi.org/data/
[6]Online. [Available]: https://crudata.uea.ac.uk/cru
[7]Online. [Available]: http://lidarradar.jpl.nasa.gov/

TABLE III
BASIC INFORMATION OF OTHER FOREST AGB MAPS USED FOR CONTRASTING

AGB Map	Region	Year	Resolution	Reference
H map	Global	2004	1 km	[57]
Z map	Global	2005	1km	[55]
T map	Northern Hemisphere	2005–2006	1 km	[58]
S map	Pan-tropic	2000	1 km	[59]
B map	Pan-tropic	2007–2008	500 m	[60]

Friedman [53], is an iterative decision tree that uses the additive model and the forward distribution algorithm to combine several weak classifiers into a strong classifier by different proportions [54]. The GRBT method has not widely used in forest AGB estimating. In this study, we used the three machine learning methods to build forest AGB estimation models. In addition, the testing dataset, which was a randomly selected 20% of the generated dataset, was used to validate these models.

The third step was mapping. Based on the training and testing results for the ANN, MARS, and GBRT algorithms, we determined the optimal models of the five different types of land cover by comparing their respective R^2 and root mean square error (RMSE) values. We used the identified optimal model and explanatory variables to generate the global forest AGB map.

C. Accuracy Assessment

In this study, we not only used the R^2 and RMSE to assess our estimated accuracy but also used a difference map and fuzzy numerical (FN) map to assess the predicted results. We used other regional and global forest AGB maps (see Table III) to do the comparison with our map. The global forest AGB map produced by Zhang and Liang [55] (subsequently called the Z map) was not yet published and was obtained through contact with the author. We calculated the difference maps from the pixel value of our forest AGB estimated map minus the corresponding pixel value of the other forest AGB maps. We derived the FN value, which represented the spatial distribution similarity of two raster maps—that is, the higher the FN value, the greater the spatial similarity of the two maps [56]. Calculating the FN value, we should choose the calculated window [56], and in order to directly compare the spatial similarity between the two maps, the window in this article was 1×1.

D. Uncertainty Analysis

In addition to the global forest AGB map, we calculated the uncertainty caused by the sample distribution uncertainty. We refer to uncertainty in terms of the standard deviation (SD) of the biomass value of the bootstrap resampling, which is often used to quantize the uncertainty of biomass estimates [35], [59], [61]. The main idea of bootstrap resampling is to have a replacement sample in the original sample to obtain new samples. Using machine learning methods to retrieve forest AGB, the training dataset would influence the results of prediction. Therefore, we should use bootstrap resampling to estimate the uncertainty caused by the spatial distribution of the training sample. In this study, we used ten bootstraps to set up biomass models, as this was considered the computation efficiency. The predicted biomass values were the average value of the ten bootstrap estimates, and the uncertainties were the SD values of the ten bootstrap estimates.

TABLE IV
APPLICATION RESULTS OF THREE MACHINE LEARNING ALGORITHMS ON EACH LAND COVER TYPE ON TRAINING DATASET

Land Cover Type	Methods	RMSE (Mg/ha)	R^2
ENF	GBRT	16.72	0.82
	ANN	18.17	0.79
	MARS	21.01	0.72
EBF	GBRT	57.11	0.71
	ANN	64.50	0.63
	MARS	75.45	0.50
DNF	GBRT	13.11	0.88
	ANN	17.42	0.78
	MARS	24.27	0.59
DBF	GBRT	27.28	0.86
	ANN	29.61	0.83
	MARS	35.50	0.76
MF	GBRT	36.95	0.77
	ANN	39.67	0.75
	MARS	47.56	0.62

III. RESULTS ANALYSIS

A. Performance of Different Machine Learning Methods

The training results for the three machine learning methods (i.e., ANN, MARS, and GBRT) across the five different types of land cover (i.e., ENF, EBF, DNF, DBF, and MF) are given in Table IV. We compared two of the statistics indexes: R^2 and RMSE. Based on a comparison of results, across the five different types of land cover in the training dataset, we found that the predictive abilities of the GBRT model were better than the other models in this study. The R^2 values, based on the GBRT model, were 0.82, 0.71, 0.88, 0.86, and 0.77 for ENF, EBF, DNF, DBF, and MF, respectively, which were higher than those for the other two models. For the five types of land cover, the RMSEs achieved by the GBRT model were also lower than the other two models for the five different types of land cover, as shown in Table IV.

The performance results for the testing dataset for ENF, EBF, DNF, DBF, and MF, based on the three machine learning methods, are presented in Table V. As for the testing dataset, the R^2 values based on the GBRT model were higher than those achieved for either the ANN model or the MARS model across the five different types of land cover at 0.79, 0.69, 0.83, 0.84, and 0.75, respectively. The RMSE values for the GBRT model also were lower than those achieved for either the ANN or the MARS models for the five different types of land cover.

A model's evaluation should consider not only its precision but also its efficiency. The computational times for the models are shown in Table VI. In this study, all the models were built on a computer with Microsoft Windows 7 system, a 3.40-GHz Intel Core and 20 GB memory. As shown in Table VI, in general,

TABLE V
APPLICATION RESULTS OF THREE MACHINE LEARNING ALGORITHMS ON EACH LAND COVER TYPE ON TESTING DATASET

Land cover type	Methods	RMSE (Mg/ha)	R^2
ENF	GBRT	17.86	0.79
	ANN	18.20	0.78
	MARS	20.76	0.71
EBF	GBRT	58.90	0.69
	ANN	63.24	0.62
	MARS	75.41	0.49
DNF	GBRT	15.63	0.83
	ANN	18.81	0.76
	MARS	24.89	0.57
DBF	GBRT	28.71	0.84
	ANN	29.98	0.82
	MARS	35.35	0.75
MF	GBRT	38.66	0.75
	ANN	39.87	0.73
	MARS	47.52	0.62

TABLE VI
MEAN ELAPSED TIME (IN SECONDS) FOR DEVELOPING A MODEL USING THE MACHINE LEARNING METHOD FOR FIVE DIFFERENT TYPES OF LAND COVER

Land cover type	Methods	Training time	Number
ENF	GBRT	7 s	654334
	MARS	34 s	
	ANN	2448 s	
EBF	GBRT	65 s	6177765
	MARS	3 s	
	ANN	291141 s	
DNF	GBRT	4 s	68017
	MARS	4 s	
	ANN	267 s	
DBF	GBRT	12 s	311741
	MARS	7 s	
	ANN	485 s	
MF	GBRT	189 s	38163620
	MARS	120 s	
	ANN	145793 s	

the GBRT model was more efficient than the ANN and MARS models, in particular, for the large training dataset. For example, the speeds of the GBRT model were within 4 min of each other, whereas the speeds of the ANN model were more than 40 min for EBF and DBF. The computational efficiencies of the GBRT models and MARS models had similar running speeds when training models with large datasets, which were better than those of the ANN models. Considering both estimation accuracy and operating efficiency, we determined the GBRT model to be relatively suitable for estimating global forest AGB in this study.

B. Global Forest AGB Mapping

After a review of the comparative results achieved by the three machine learning methods on the five different types of land cover, the final map of the global forest AGB estimation was derived from the GBRT model. To compare this map with the other forest AGB maps listed in Table III, we produced a global forest AGB map using input variables applicable to the year 2005. Fig. 2(a) shows the spatial distribution of the global forest AGB estimated map with a mean biomass density

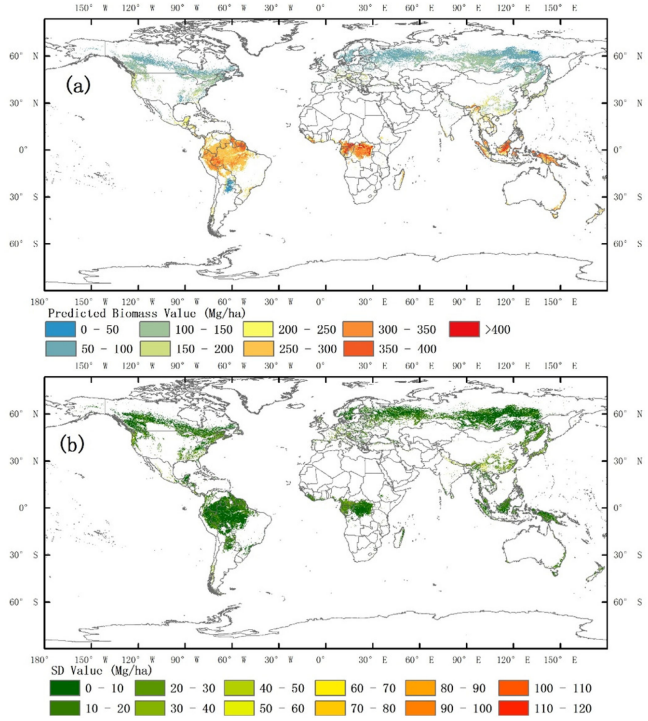

Fig. 2. (a) Global forest AGB map based on GBRT models for 2005. (b) Absolute uncertainty induced by training sample distribution uncertainty.

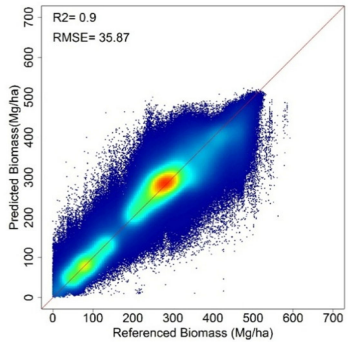

Fig. 3. Predicted biomass against referenced biomass data.

of 174.33 Mg/ha. As shown in Fig. 2(a), the maximum value for forest AGB appeared in the pan-tropical forest area, whereas a relatively low forest AGB value was achieved by the boreal forest area, which is situated primarily in North America and Eurasia.

We assessed the uncertainty of the AGB estimation, caused by the training sample distribution uncertainty, using the SD from the ten bootstrap samples and gave the value of 11.95 Mg/ha. As shown in Fig. 2(b), the value of the overall uncertainty was not large, but it was still relatively high in some regions. For example, in southern China and parts of the tropical forest area where the biomass density was high, the value of the uncertainty was larger than 20 Mg/ha.

In this study, we randomly selected 20% of the reference data for validation, as shown in Fig. 3. The predicted forest AGB map was fitted relatively well with the reference data that the R^2 value between the estimated and reference AGB was 0.90

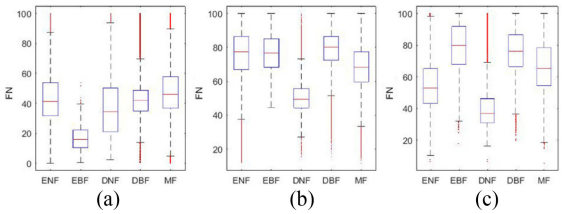

Fig. 4. Box plots of FN for North America forest areas comparing our estimated map with (a) T map, (b) H map, and (c) Z map.

and the RMSE was 35.87 Mg/ha. Compared with numerous studies using LiDAR wavelength data and field data to establish an estimated model, the accuracy of this study was comparable. Additionally, the data processing aspect of this study was easier than direct use of LiDAR data, and it can improve the efficiency of estimation. Additionally, this method mainly relied on high-level remote sensing data. Therefore, it has the ability to produce time series of high-resolution global forest AGB maps.

C. Comparison With Other Regional Forest AGB

To further evaluate our results, we compared our estimated forest AGB map with other AGB maps covering various areas. We used the FN value to analyze the spatial differences between our AGB map and others based on diverse forest types and used difference maps to evaluate these comparisons.

1) North America: For North America, we used forest AGB maps derived by Thurner *et al*. [58] (the T map), Hu *et al*. [57] (the H map), and Zhang and Liang [55] (the Z map) for comparison with our *forest AGB map.*

The FN value between our AGB and H and that between our map and Z map was high [see Fig. 4(b) and (c)], whereas the FN value between our AGB and T map was relatively low [see Fig. 4(a)], which means the spatial distribution between our AGB map and T map has large difference. As shown in Fig. 5(a), our map gave higher values than the T map, which may have been caused by the growing stock volume (GSV) data they used, which were derived from SAR [13]. They used the GSV data to derive biomass reached saturation with high GSV values (>300 m^3/ha), which resulted in lower AGB estimates than others.

Compared with H and Z maps, as shown in Fig. 4(b) and (c), the FN value of DNF type was lower than other forest types (ENF, EBF, DBF, and MF). In North America, DNF was mainly distributed at high altitudes with low biomass density, whereas the DNF estimation model in this study did not fit well on low biomass density. However, the main forest types in North America were ENF and MF. The FN value of ENF type between our AGB and H map was mainly ranged from 66.90 to 86.55, and that between our AGB and Z map was ranged from 43.13 to 65.22. The FN value of MF type between our AGB map and these two maps, H and Z maps, were relatively high, as shown in Fig. 4(b) and (c). This indicated that these two forest AGB maps, the H and Z maps, were similar to our forest AGB map on spatial distribution. However, the absolute value of our AGB map exhibited slightly lower values than these two maps [see Fig. 5(b) and (c)], and the average differences between our map and the

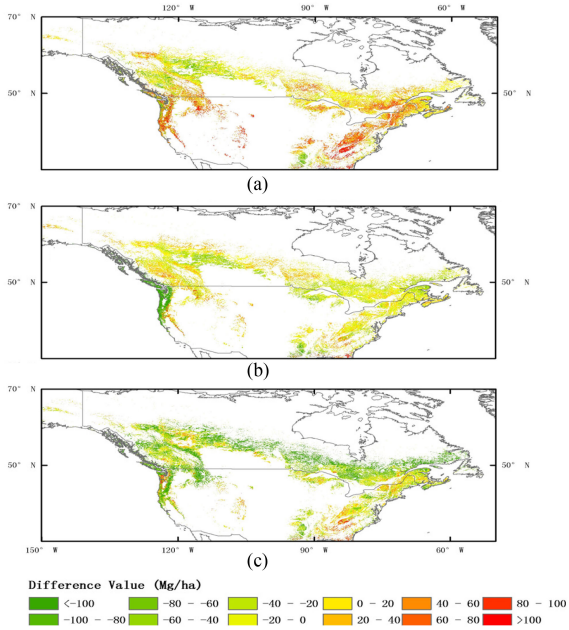

Fig. 5. Difference maps for North America forest areas comparing our estimated map with (a) T map (our forest AGB map minus T map), (b) H map (our forest AGB map minus H map), and (c) Z map (our map minus Z map).

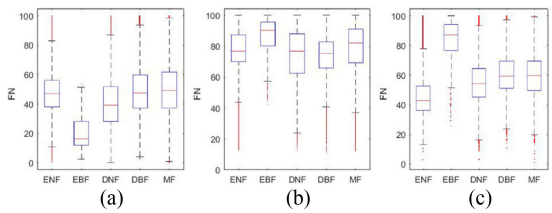

Fig. 6. Box plots of FN for northern Eurasia forest areas comparing our estimated map with (a) T map, (b) H map, and (c) Z map.

H map and the Z map were −50.03 Mg/ha and −70.22 Mg/ha, respectively.

2) Eurasia: Due to the underestimation of T map, in Eurasia, the spatial distribution of our AGB was less similar to that of T map [see Fig. 6(a)], the mean difference between our map and the T map was 51.91 Mg/ha, and the relative error was 41.59% [see Fig. 7(a)].

In Eurasia, the main forest types were MF and DNF. On these two forest types, the spatial distribution of our AGB was relatively similar to that of the H map, because the FN value of MF and DNF types was ranged from 69.35 to 91.01 and 62.43 to 88.09, respectively, as shown in Fig. 6(b). However, there were still some distinctions between our map and H map. In southern Russia, the value of our estimated AGB was higher than that of H map. Whereas as a whole, the mean difference value between our predicted value and the H map was −21.56 Mg/ha, and the relative error was 15.63% [see Fig. 7(b)]. Hu *et al*. [57] used field data, auxiliary data, and extrapolated GLAS waveform data to establish a random forest model to estimate the forest AGB. The field data they used, however, were unevenly distributed in the Eurasian region [62]. The use of extrapolated GLAS waveform data also could lead to certain errors. Therefore, the

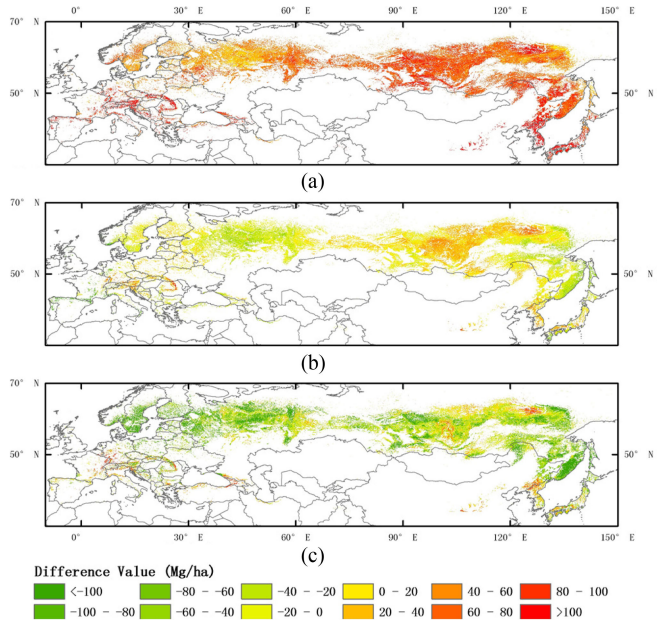

Fig. 7. Difference maps for northern Eurasia forest areas comparing our estimated map with (a) T map (our forest AGB map minus T map), (b) H map (our forest AGB map minus H map), and (c) Z map (our map minus Z map).

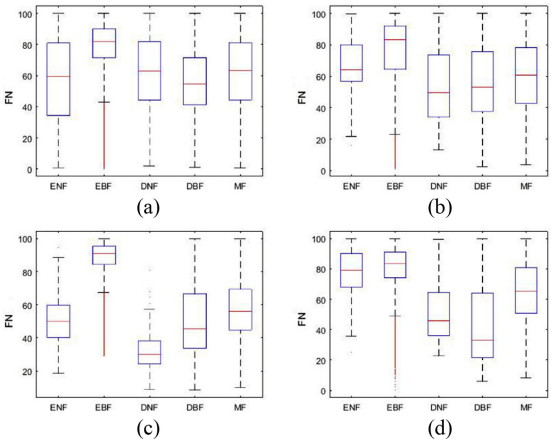

Fig. 8. Box plots of FN for pan-tropical forest areas comparing our estimated map with (a) S map, (b) B map, (c) H map, and (d) the Z map.

estimated results in some parts of Eurasia in the H map had a lot of uncertainty. In the Tin Holt Mountains region of Russia, our estimated AGB map and the Z map have some significant differences [see Fig. 7(c)], and the forest AGB estimated in this study in the western part of Russia was smaller than the Z map. In the Eurasian region, the mean difference between our estimation AGB map and the Z map was −74.45 Mg/ha, which may be caused by using different reference data.

3) Pan-Tropical Forests: In pan-tropical forest areas, the main forest type was EBF, followed by DBF, whereas other forest types were less. As shown in Fig. 8, for EBF type, the FN value between our AGB map and the AGB estimated from [59] (S map) and [60] (B map), H map, and Z map was relatively high, and the main ranges of FN value were 71.34–90.23, 64.39–92.04, 84.28–95.53, 74.15–91.08, respectively. For other forest types, there were some differences in spatial distribution

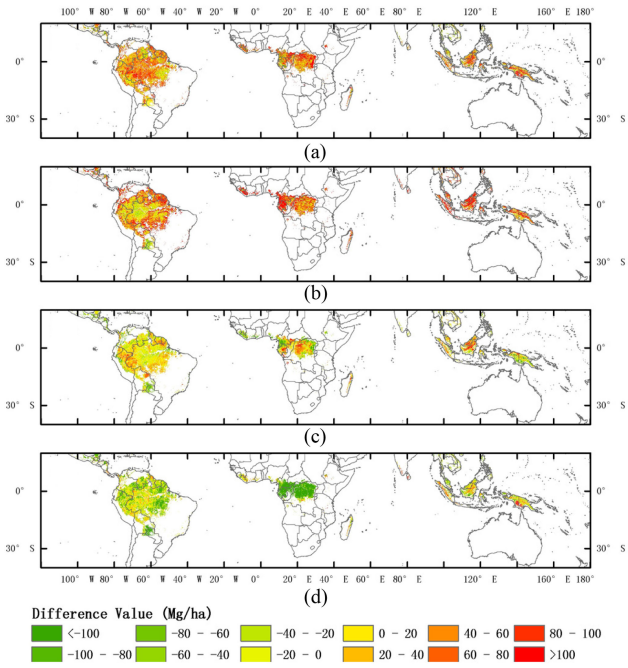

Fig. 9. Difference maps comparing our estimated map for pan-tropical forest areas and (a) S map (our map minus S map), (b) B map (our map minus B map), (c) H map (our map minus H map), and (d) Z map (our map minus Z map).

between our AGB map and S, B, H, Z maps. For DBF type, the FN value between our estimated AGB and that from H map and Z map was relatively low. It indicated that the spatial distribution similarity between them was small. In the pan-tropical region, DBF was mainly distributed in southeastern Bolivia, western Paraguay, northern Argentina, and near the Peruvian Andes. Due to the limitation available field or plot data, the complexity of the geographical environment in these regions, and the different data sources of varied products, there were significant distinctions between different products in these regions, as shown in Fig. 9.

As shown in Fig. 9(a) and (b), results from our predicted map were slightly higher than that of the S and B maps. The main difference between our estimated AGB map and the S map appeared in northwest Brazil and the northeastern part of the Congo [see Fig. 9(a)]. Overall, the mean difference value between our AGB map and S map was 52.91Mg/ha. In addition, our AGB density was higher than that of the B map, and the large difference values mainly situated in Paraguay and the Gabonese region of central and western Africa, as shown in Fig. 9(b). In general, the averaged difference between our estimated AGB map and the B map was 75.07 Mg/ha, which was similar to the results shown in Mitchard, *et al.* [63]. Mitchard, *et al.* [63] assessed B map by using lots of field data and indicated the B map was underestimated. In addition, the value of our estimated forest AGB map was slightly lower than the Z map [see Fig. 9(d)], especially in the Congo Basin. The average difference value between the Z map and our estimated map was −70.30 Mg/ha. This may be caused by using different data. However, compared with other products, the difference between our estimated AGB map and the H map was relatively small at −21.87 Mg/ha [see Fig. 9(c)].

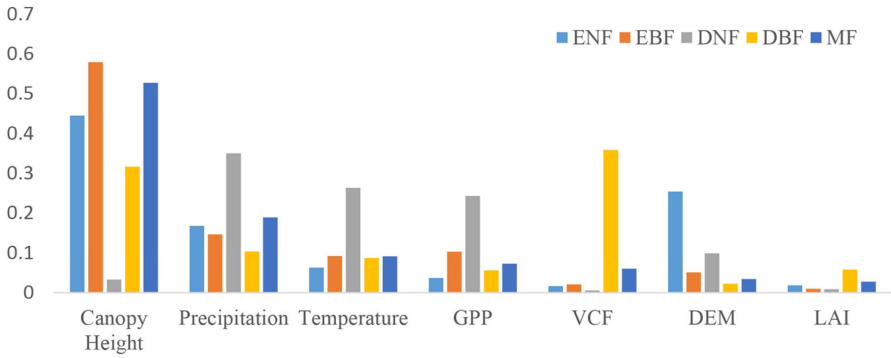

Fig. 10. Relative importance of variables to the AGB estimation GBRT model built from the training dataset. Variables included monthly total precipitation and mean temperature, height, DEM, monthly total GPP, annual mean VCF, and monthly maximum LAI.

IV. Discussion

A. Relative Importance of Variables

In estimating global forest AGB, we discussed the relative importance of variables, and this showed how valuable each variable was in the construction of the boosted decision trees within the model. After we built the GBRT models, it was relatively simple to obtain importance scores for each predicted variables, because a trained GBRT model can automatically calculate the importance of variables. Technical information on how variables' importance can be calculated in boosted decision trees can be found in [64].

In this study, the variables used in the estimation of global forest AGB included monthly total precipitation, monthly mean temperature, tree height, DEM, annual maximum LAI, monthly total GPP, and annual mean VCF. As shown in Fig. 10, generally, canopy height was the most important variable in estimating global forest AGB, followed by precipitation and temperature. The other variables contributed less in estimating forest AGB in this study. This conclusion was similar to most research results that showed canopy height has a strong correlation with forest AGB, and it is an important parameter for estimating forest AGB [21], [49], especially for areas with high biomass density [22], [23], such as pan-tropical forest areas, where ENF was mainly distributed.

Precipitation and temperature can be summarized as meteorological factors. For forest AGB, meteorological factors would affect plant growth and carbon sequestration capacity [15], [65]. In other words, precipitation can provide water and energy for plants growth, and temperature can affect the sequestration capacity of plants by affecting photosynthesis [19]. In addition, the temperature would also affect the respiration rate of plants and, thus, affecting the energy consumption of plants. Therefore, precipitation and temperature were important variables used to estimate forest AGB. As shown in Fig. 10, for DNF type, meteorological factors were the most important estimation factors, as DNF was mainly distributed at high latitudes, with relatively flat terrain and low biomass density.

Other variables used in this study, such as GPP, LAI, and VCF, described the horizontal structural information of forests, which may correlate with precipitation and temperature. Hence, these variables had a smaller contribution in estimating forest AGB. The best estimation results were obtained only by using all variables.

We also analyzed the relative importance of variables for the AGB-estimated GBRT model at a regional scale. As shown in Fig. 11, precipitation was the most important variable for the AGB-estimated GBRT model built from the training dataset in North America. Additionally, precipitation and temperature provided the main information for the estimated GBRT model in Eurasia. This indicated that the climate factors were the most important variables for the AGB-estimated GBRT model in the Northern Hemisphere. The forest in the Northern Hemisphere was the primary mature forest, and the climate was the primary controlling factor for AGB [33]. In China, most forests were relatively young [66], which were still in the growing stage; therefore, as shown in Fig. 11(c), canopy height was the most important estimation factor. Additionally, in Brazil, high regional forest biomass density and vertical information of forest structure (canopy height) gave more information than other variables for estimating AGB, as shown in Fig. 11(d). On the whole, the relative importance of variables is different in different regions.

B. Limitations of the Current Study

In this study, the global forest AGB map retrieved by the GBRT model showed good precision compared with independent reference data and other forest AGB maps; however, room for improvement still remains.

Currently, we used several LiDAR-generated biomass maps (see Table II), which were retrieved by establishing the relationship between LiDAR waveform data and field data to estimate forest AGB. Although we chose the pixels that had relatively low uncertainty ($<10\%$) as the reference data, there was still a certain degree of error.

In addition, since the field data collection year did not exactly match the year of LiDAR-generated biomass data, the calibration process, using the field data to establish a regression relationship with LiDAR-generated biomass data to correct the LiDAR-generated biomass data, produced some errors because the growth of the AGB during this time was not considered.

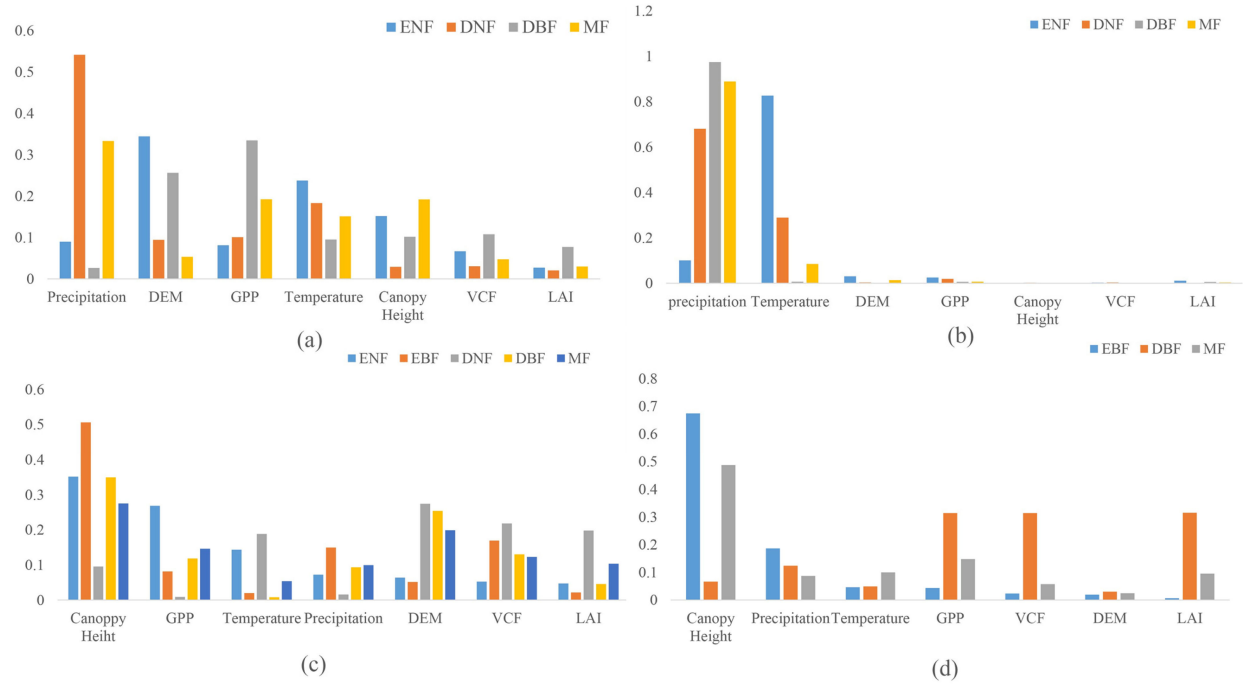

Fig. 11. Relative importance of variables to the regional AGB estimation GBRT model built from the training dataset in (a) North America, (b) Eurasia, (c) China, and (d) Brazil. Variables included monthly total precipitation and mean temperature, height, DEM, monthly total GPP, annual mean VCF, and monthly maximum LAI.

In this study, the average value of field data with the same geographic location but with different collected times was taken as the true value of the corresponding forest AGB. This may reduce the error associated with forest AGB growth, but it would be smaller if more field data could be collected.

Furthermore, in the process of establishing a relationship between the reference data and other variables (e.g., LAI, GPP, VCF, and precipitation), we may have produced geographical matching errors, which could have affected the accuracy of the final biomass map. Additionally, in the current study, uncertainties may have been introduced by other variables (e.g., LAI, GPP, and VCF). These potential sources of error need to be considered in future forest AGB estimation studies. Additionally, if high-quality LiDAR-derived biomass data can be collected to estimate global forest AGB, accuracy may be improved.

V. Conclusion

In this study, we developed a method to estimate global forest AGB by integrating the LiDAR-derived forest AGB datasets, field measurements, high-level products from optical satellite data, and other ancillary data. We selected the optimal algorithm, GBRT, after comparing AGB estimation and the computational efficiencies from three machine learning methods. We generated the 2005 global forest AGB map using the optimal algorithm. The mean value of the global forest AGB in 2005 was 174.33 Mg/ha. The mean uncertainty caused by training sample distribution uncertainty was 11.95 Mg/ha. The R^2 of validation with independent reference data was 0.90 and that of RMSE was 35.87 Mg/ha. The contrast results between our forest AGB map and other maps showed good consistency in spatial distribution. Furthermore, the variables used in this study were almost time continuous, making it possible to produce continuous forest AGB maps, which may contribute to global carbon and environmental research. In this study, we produced a 2005 global forest AGB map. Our method may be easily applied to generate time-series maps. Further research should explore temporal changes in global forest AGB.

Acknowledgment

The authors would like to thank anonymous reviewers for their constructive comments and suggestions. The authors would also like to thank the GLASS science team, the MODIS science team (https://modis.gsfc.nasa.gov), NASA and the National Geospatial-Intelligence Agency (http://www.cgiar-csi.org/data/srtm-90m-digital-elevation-database-v4-1), the CRU science team (https://crudata.uea.ac.uk/cru), the NCEI science team (https://www.ncei.noaa.gov/), and the JPL science team (http://lidarradar.jpl.nasa.gov/). This new biomass map is publically available free of charge at http://www.glass.umd.edu or http://www.geodata.cn.

References

[1] Y. Pan *et al.*, "A large and persistent carbon sink in the world's forests," *Science*, vol. 333, no. 6045, pp. 988–993, 2011.

[2] J. Chave *et al.*, "Tree allometry and improved estimation of carbon stocks and balance in tropical forests," *Oecologia*, vol. 145, no. 1, pp. 87–99, 2005.

[3] C. Huang *et al.*, "An automated approach for reconstructing recent forest disturbance history using dense Landsat time series stacks," *Remote Sens. Environ.*, vol. 114, no. 1, pp. 183–198, 2010.

[4] V. Avitabile, M. Herold, M. Henry, and C. Schmullius, "Mapping biomass with remote sensing: A comparison of methods for the case study of Uganda," *Carbon Balance Manage.*, vol. 6, 2011, Art. no. 7.

[5] D. Lu, "The potential and challenge of remote sensing-based biomass estimation," *Int. J. Remote Sens.*, vol. 27, no. 7, pp. 1297–1328, 2006.

[6] H. Klinge, W. Rodrigues, E. Brunig, and E. Fittkau, "Biomass and structure in a central Amazonian rain forest," in *Tropical Ecological Systems*. Berlin, Germany: Springer, 1975, pp. 115–122.

[7] M. K. Steininger, "Satellite estimation of tropical secondary forest aboveground biomass: Data from Brazil and Bolivia," *Int. J. Remote Sens.*, vol. 21, no. 6/7, pp. 1139–1157, 2000.

[8] J. Dong *et al.*, "Remote sensing estimates of boreal and temperate forest woody biomass: Carbon pools, sources, and sinks," *Remote Sens. Environ.*, vol. 84, no. 3, pp. 393–410, 2003.

[9] M. Segura and M. Kanninen, "Allometric models for tree volume and total aboveground biomass in a tropical humid forest in Costa Rica," *Biotropica*, vol. 37, no. 1, pp. 2–8, 2005.

[10] B.-L. Xue *et al.*, "Evaluation of modeled global vegetation carbon dynamics: Analysis based on global carbon flux and above-ground biomass data," *Ecol. Model.*, vol. 355, pp. 84–96, 2017.

[11] K. Lim, P. Treitz, M. Wulder, B. Stonge, and M. Flood, "LiDAR remote sensing of forest structure," *Prog. Phys. Geogr.*, vol. 27, no. 1, pp. 88–106, 2003.

[12] D. Lu, "Aboveground biomass estimation using Landsat TM data in the Brazilian Amazon," *Int. J. Remote Sens.*, vol. 26, no. 12, pp. 2509–2525, 2007.

[13] M. Santoro *et al.*, "Retrieval of growing stock volume in boreal forest using hyper-temporal series of Envisat ASAR ScanSAR backscatter measurements," *Remote Sens. Environ.*, vol. 115, no. 2, pp. 490–507, 2011.

[14] W. Qi and R. O. Dubayah, "Combining tandem-X InSAR and simulated GEDI lidar observations for forest structure mapping," *Remote Sens. Environ.*, vol. 187, pp. 253–266, 2016.

[15] A. McGuire *et al.*, "Carbon balance of the terrestrial biosphere in the twentieth century: Analyses of CO_2, climate and land use effects with four process-based ecosystem models," *Global Biogeochem. Cycles*, vol. 15, no. 1, pp. 183–206, 2001.

[16] V. Arora, "Modeling vegetation as a dynamic component in soil-vegetation-atmosphere transfer schemes and hydrological models," *Rev. Geophys.*, vol. 40, no. 2, pp. 1–26, 2002.

[17] X. Zhang and S. Kondragunta, "Estimating forest biomass in the USA using generalized allometric models and MODIS land products," *Geophys. Res. Lett.*, vol. 33, pp. 1–5, 2006.

[18] G. Zhang *et al.*, "Estimation of forest aboveground biomass in California using canopy height and leaf area index estimated from satellite data," *Remote Sens. Environ.*, vol. 151, pp. 44–56, 2014.

[19] R. H. Whittaker and G. E. Likens, "Carbon in the biota," in *Carbon and the Biosphere: Proc. 24th Brookhaven Symp. Biol.*, G. M. Woodwell, E. V. Pecan, Eds., 1973, pp. 281–302.

[20] H. C. Keeling and O. L. Phillips, "The global relationship between forest productivity and biomass," *Global Ecol. Biogeogr.*, vol. 16, no. 5, pp. 618–631, 2007.

[21] Q. Molto *et al.*, "Predicting tree heights for biomass estimates in tropical forests," *Biogeosciences*, vol. 10, no. 5, pp. 8611–8635, 2013.

[22] R. O. Dubayah *et al.*, "Estimation of tropical forest height and biomass dynamics using lidar remote sensing at La Selva, Costa Rica," *J. Geophys. Res. Biogeosci.*, vol. 115, no. G2, pp. 272–281, 2015.

[23] T. R. Feldpausch and S. J. Lloyd, "Tree height integrated into pantropical forest biomass estimates," *Biogeosciences*, vol. 9, pp. 3381–3403, 2012.

[24] Y. Pan, R. A. Birdsey, O. L. Phillips, and R. B. Jackson, "The structure, distribution, and biomass of the world's forests," *Annu. Rev. Ecol., Evol., Systematics*, vol. 44, no. 1, pp. 593–622, 2013.

[25] C. V. de Castilho *et al.*, "Variation in aboveground tree live biomass in a central Amazonian Forest: Effects of soil and topography," *Forest Ecol. Manage.*, vol. 234, no. 1/3, pp. 85–96, 2006.

[26] H. A. Margolis *et al.*, "Combining satellite lidar, airborne lidar, and ground plots to estimate the amount and distribution of aboveground biomass in the boreal forest of North America," *Can. J. Forest Res.*, vol. 45, no. 7, pp. 838–855, 2015.

[27] C. Neigh *et al.*, "LiDAR-based biomass estimates, boreal forest biome, Eurasia, 2005–2006," ORNL DAAC, Oak Ridge, TN, USA, 2015. Available. [Online]: http://dx.doi.org/10.3334/ORNLDAAC/1278

[28] V. Avitabile *et al.*, "An integrated pan-tropical biomass map using multiple reference datasets," *Global Change Biol.*, vol. 22, no. 4, pp. 1406–20, Apr. 2016.

[29] S. L. Lewis *et al.*, "Above-ground biomass and structure of 260 African tropical forests," *Philos. Trans. Roy. Soc. London B, Biol. Sci.*, vol. 368, no. 1625, 2013, Art. no. 20120295.

[30] E. T. A. Mitchard *et al.*, "Markedly divergent estimates of Amazon forest carbon density from ground plots and satellites," *Global Ecol. Biogeogr.*, vol. 23, no. 8, pp. 935–946, 2014.

[31] M. J. P. Sullivan *et al.*, "Diversity and carbon storage across the tropical forest biome," *Sci. Rep.*, vol. 7, 2017, Art. no. 39102.

[32] D. Schepaschenko *et al.*, "A dataset of forest biomass structure for Eurasia," *Sci. Data*, vol. 4, 2017, Art. no. 170070.

[33] Y. Liu, G. Yu, Q. Wang, and Y. Zhang, "How temperature, precipitation and stand age control the biomass carbon density of global mature forests," *Global Ecol. Biogeogr.*, vol. 23, no. 3, pp. 323–333, 2014.

[34] Z. Ma *et al.*, "Regional drought-induced reduction in the biomass carbon sink of Canada's boreal forests," *Proc. Nat. Acad. Sci. USA*, vol. 109, no. 7, pp. 2423–2427, Feb. 14 2012.

[35] Y. Su *et al.*, "Spatial distribution of forest aboveground biomass in China: Estimation through combination of spaceborne lidar, optical imagery, and forest inventory data," *Remote Sens. Environ.*, vol. 173, pp. 187–199, 2016.

[36] V. Avitabile and A. Camia, "An assessment of forest biomass maps in Europe using harmonized national statistics and inventory plots," *Forest Ecol. Manage.*, vol. 409, pp. 489–498, 2018.

[37] S. Liang *et al.*, in *Global Land Surface Satellite (GLASS) Products: Algorithms, Validation and Analysis (SpringerBriefs in Earth Sciences).* Berlin, Germany: Springer, 2013.

[38] S. Liang *et al.*, "A long-term Global LAnd Surface Satellite (GLASS) data-set for environmental studies," *Int. J. Digit. Earth*, vol. 6, pp. 5–33, 2013.

[39] Z. Xiao *et al.*, "Long-time-series global land surface satellite leaf area index product derived from MODIS and AVHRR surface reflectance," *IEEE Trans. Geosci. Remote Sens.*, vol. 54, no. 9, pp. 5301–5318, Sep. 2016.

[40] Z. Xiao, S. Liang, and B. Jiang, "Evaluation of four long time-series global leaf area index products," *Agric. Forest Meteorol.*, vol. 246, pp. 218–230, 2017.

[41] B. Xu *et al.*, "An integrated method for validating long-term leaf area index products using global networks of site-based measurements," *Remote Sens. Environ.*, vol. 209, pp. 134–151, 2018.

[42] W. Yuan *et al.*, "Global estimates of evapotranspiration and gross primary production based on MODIS and global meteorology data," *Remote Sens. Environ.*, vol. 114, no. 7, pp. 1416–1431, 2010.

[43] Y. Zhang and S. Liang, "Surface radiative forcing of forest disturbances over northeastern China," *Environ. Res. Lett.*, vol. 9, no. 2, pp. 69–75, 2014.

[44] J. Ma, X. Yan, W. Dong, and J. Chou, "Gross primary production of global forest ecosystems has been overestimated," *Sci. Rep.*, vol. 5, 2015, Art. no. 10820.

[45] T. Xu, S. M. Bateni, S. Liang, D. Entekhabi, and K. Mao, "Estimation of surface turbulent heat fluxes via variational assimilation of sequences of land surface temperatures from Geostationary Operational Environmental Satellites," *J. Geophys. Res. Atmos.*, vol. 119, no. 18, pp. 10780–10798, 2015.

[46] A. Jarvis, H. I. Reuter, A. Nelson, and E. Guevara, "Hole-filled SRTM for the globe version 4," Available from the CGIAR-CSI SRTM 90 m Database," 2008.

[47] J. R. Thompson, D. R. Foster, R. Scheller, and D. Kittredge, "The influence of land use and climate change on forest biomass and composition in Massachusetts, USA," *Ecol. Appl.*, vol. 21, no. 7, pp. 2425–2444, 2011.

[48] I. Harris, P. D. Jones, T. J. Osborn, and D. H. Lister, "Updated high-resolution grids of monthly climatic observations—The CRU TS3.10 Dataset," *Int. J. Climatol.*, vol. 34, no. 3, pp. 623–642, 2014.

[49] M. Simard, N. Pinto, J. B. Fisher, and A. Baccini, "Mapping forest canopy height globally with spaceborne lidar," *J. Geophysical Res.: Biogeosci.*, vol. 116, no. G 4021, pp. 1–12, 2011.

[50] R. Vidal, Y. Ma, and S. S. Sastry, "Principal component analysis," *IEEE Trans. Pattern Anal. Mach. Intell.*, vol. 27, no. 12, pp. 1945–1959, 2005.

[51] A. M. Filippi, İ. Güneralp, and J. Randall, "Hyperspectral remote sensing of aboveground biomass on a river meander bend using multivariate adaptive regression splines and stochastic gradient boosting," *Remote Sens. Lett.*, vol. 5, no. 5, pp. 432–441, 2014.

[52] I. Ali, F. Greifeneder, J. Stamenkovic, M. Neumann, and C. Notarnicola, "Review of machine learning approaches for biomass and soil moisture retrievals from remote sensing data," *Remote Sens.*, vol. 7, no. 12, pp. 16398–16421, 2015.

[53] J. H. Friedman, "Greedy function approximation: A gradient boosting machine," *Ann. Statist.*, vol. 29, no. 5, pp. 1189–1232, 2001.

[54] L. Yang *et al.*, "Estimating surface downward shortwave radiation over China based on the gradient boosting decision tree method," *Remote Sens.*, vol. 10, no. 2, 2018, Art. no. 185.
[55] Y. Zhang S. Liang, and L. Yang, "A review of regional and global gridded forest biomass datasets," *Remote Sens.*, vol. 11, 2019, Art. no. 2744.
[56] A. Hagen-Zanker, "Comparing continuous valued raster data: A cross disciplinary literature scan," Research Institute for Knowledge Systems, Maastricht, The Netherlands, 2006.
[57] T. Hu *et al.*, "Mapping global forest aboveground biomass with spaceborne LiDAR, optical imagery, and forest inventory data," *Remote Sens.*, vol. 8, no. 7, 2016, Art. no. 565.
[58] M. Thurner *et al.*, "Carbon stock and density of northern boreal and temperate forests," *Global Ecol. Biogeogr.*, vol. 23, no. 3, pp. 297–310, 2014.
[59] S. S. Saatchi *et al.*, "Benchmark map of forest carbon stocks in tropical regions across three continents," *Proc. Nat. Acad. Sci. USA*, vol. 108, no. 24, pp. 9899–904, 2011.
[60] A. Baccini, N. Laporte, S. J. Goetz, M. Sun, and H. Dong, "A first map of tropical Africa's above-ground biomass derived from satellite imagery," *Environ. Res. Lett.*, vol. 3, no. 4, pp. 45011–45019, 2008.
[61] Y. Zhang, S. Liang, and G. Sun, "Forest biomass mapping of northeastern china using GLAS and MODIS Data," *IEEE J. Sel. Topics Appl. Earth Observ. Remote Sens.*, vol. 7, no. 1, pp. 140–152, Jan. 2014.
[62] P. Rodríguez-Veiga *et al.*, "Forest biomass retrieval approaches from earth observation in different biomes," *Int. J. Appl. Earth Observ. Geoinf.*, vol. 77, pp. 53–68, 2019.
[63] E. T. A. Mitchard *et al.*, "Comment on 'A first map of tropical Africa's above-ground biomass derived from satellite imagery'," *Environ. Res. Lett.*, vol. 6, no. 4, 2011, Art. no. 049001.
[64] D. Ruppert, "The elements of statistical learning: Data mining, inference, and prediction," *Math. Intell.*, vol. 99, no. 466, pp. 567–567, 2010.
[65] F. I. Woodward, M. R. Lomas, and C. K. Kelly, "Global climate and the distribution of plant biomes," *Philos. Trans. Roy. Soc. London B, Biol. Sci.*, vol. 359, no. 1450, pp. 1465–1476, 2004.
[66] Y. Zhang, Y. Yao, X. Wang, Y. Liu, and S. Piao, "Mapping spatial distribution of forest age in China," *Earth Space Sci.*, vol. 4, no. 3, pp. 108–116, 2017.

Lu Yang received the M.Sc. degree in geography from Beijing Normal University, Beijing, China, in 2019. She is currently working toward the Ph.D. degree at Peking University, Beijing, China.

Her research interests include forest biomass mapping from multisource remote sensing data and the impact of urbanization on biomass.

Shunlin Liang (Fellow, IEEE) received the Ph.D. degree in geography from Boston University, Boston, MA, USA, in 1993.

He is currently a Professor with the Department of Geographical Sciences, University of Maryland, College Park, MD, USA. He has authored/coauthored more than 360 SCI indexed peer-reviewed journal papers, 42 book chapters, and nine special issues of different journals and has authored/edited seven books, four of which were translated in Chinese, such as *Quantitative Remote Sensing of Land Surfaces* (Wiley, 2004), *Advances in Land Remote Sensing: System, Modeling, Inversion and Application* (Springer, 2008), *Advanced Remote Sensing: Terrestrial Information Extraction and Applications* (Academic Press, 2012 and 2019), *Global LAnd Surface Satellite (GLASS) Products: Algorithms, Validation and Analysis* (Springer, 2013), *Land Surface Observation, Modeling, Data Assimilation (World Scientific, 2013),* and *Earth's Energy Budget* (Elsevier, 2017). He was the Editor-in-Chief for the nine-volume books entitled *Comprehensive Remote Sensing* (Elsevier, 2017). His main research interests include the estimation of land surface variables from satellite data, earth's energy balance, and assessment of environmental changes.

Dr. Liang was an Associate Editor for the IEEE TRANSACTION ON GEOSCIENCE AND REMOTE SENSING and is currently an Editor-in-Chief of *Science of Remote Sensing.*

Yuzhen Zhang received the Ph.D. degree in global environmental change from Beijing Normal University, Beijing, China, in 2014.

She is currently an Associate Professor with the School of Automation and Electrical Engineering, University of Science and Technology Beijing, Beijing, China. Her main research interests include forest biomass mapping from lidar, optical and radar data, assessing the impact of climate and disturbances on forest biomass dynamics, and exploring the climatic effects of forest disturbances and land use land cover changes.